

Nanoboomerang-based inverse metasurfaces—A promising path towards ultrathin photonic devices for transmission operation

Cite as: APL Photonics 2, 036102 (2017); <https://doi.org/10.1063/1.4974343>

Submitted: 13 October 2016 . Accepted: 07 January 2017 . Published Online: 06 February 2017

Matthias Zeisberger, Henrik Schneidewind , Uwe Huebner, Juergen Popp, and Markus A. Schmidt



View Online



Export Citation



CrossMark

ARTICLES YOU MAY BE INTERESTED IN

[Ultra-compact visible chiral spectrometer with meta-lenses](#)

APL Photonics 2, 036103 (2017); <https://doi.org/10.1063/1.4974259>

[Invited Article: Broadband highly efficient dielectric metadevices for polarization control](#)

APL Photonics 1, 030801 (2016); <https://doi.org/10.1063/1.4949007>

[Why I am optimistic about the silicon-photonic route to quantum computing](#)

APL Photonics 2, 030901 (2017); <https://doi.org/10.1063/1.4976737>

additive manufacturing epitaxial crystal growth cerium oxide polishing powder silver nanoparticles sputtering targets III-IV semiconductors CVD precursors europium phosphors

AMERICAN ELEMENTS

THE ADVANCED MATERIALS MANUFACTURER®

deposition slugs OLED Lighting spintronics solar energy osmium nanoribbons thin films chalcogenides AuNPs GDC Li-ion battery electrolytes 99.999% ruthenium spheres

endoheedral fullerenes copper nanoparticles diamond micropowder CIGS MBE grade materials palladium catalysts flexible electronics beta-barium borate borosilicate glass dysprosium pellets YBCO pyrolytic graphite 3d graphene foam indium tin oxide mesoporous silica raman substrates sapphire windows tungsten carbide InGaAs barium fluoride carbon nanotubes lithium niobate scandium powder

gallium lump glassy carbon nanodispersions InAs wafers laser crystals ultra high purity materials MOFs surface functionalized nanoparticles organometallics quantum dot Al Si P S Cl Ar rare earth metals photovoltaics refractory metals MOCVD superconductors transparent ceramics ultra high purity silicon

American Elements opens up a world of possibilities so you can **Now Invent!**

Over 15,000 certified high purity laboratory chemicals, metals, & advanced materials and a state-of-the-art Research Center. Printable GHS-compliant Safety Data Sheets. Thousands of new products. And much more. All on a secure multi-language "Mobile Responsive" platform.

perovskite crystals yttrium iron garnet alternative energy h-BN gold nanocubes graphene oxide macromolecules photonics rhodium sponge fiber optics beamsplitters infrared dyes zeolites fused quartz metallocenes platinum ink buckyballs Ti-6Al-4V

Now Invent.™
The Next Generation of Material Science Catalogs

www.americanelements.com



Nanoboomerang-based inverse metasurfaces—A promising path towards ultrathin photonic devices for transmission operation

Matthias Zeisberger,¹ Henrik Schneidewind,^{1,a} Uwe Huebner,¹ Juergen Popp,¹ and Markus A. Schmidt^{1,2,3}

¹Leibniz Institute of Photonic Technology e.V., 07745 Jena, Germany

²Otto Schott Institute of Material Research, Friedrich-Schiller-University, 07743 Jena, Germany

³Abbe Center of Photonics, Friedrich-Schiller-University, 07743 Jena, Germany

(Received 13 October 2016; accepted 7 January 2017; published online 6 February 2017)

Metasurfaces have revolutionized photonics due to their ability to shape phase fronts as requested and to tune beam directionality using nanoscale metallic or dielectric scatterers. Here we reveal inverse metasurfaces showing superior properties compared to their positive counterparts if transmission mode operation is considered. The key advantage of such slot-type metasurfaces is the strong reduction of light in the parallel-polarization state, making the crossed-polarization, being essential for metasurface operation, dominant and highly visible. In the experiment, we show an up to four times improvement in polarization extinction for the individual metasurface element geometry consisting of deep subwavelength nanoboomerangs with feature sizes of the order of 100 nm. As confirmed by simulations, strong plasmonic hybridization yields two spectrally separated plasmonic resonances, ultimately allowing for the desired phase and scattering engineering in transmission. Due to the design flexibility of inverse metasurfaces, a large number of highly integrated ultra-flat photonic elements can be envisioned, examples of which include monolithic lenses for telecommunications and spectroscopy, beam shaper or generator for particle trapping or acceleration or sophisticated polarization control for microscopy. © 2017 Author(s). All article content, except where otherwise noted, is licensed under a Creative Commons Attribution (CC BY) license (<http://creativecommons.org/licenses/by/4.0/>). [<http://dx.doi.org/10.1063/1.4974343>]

INTRODUCTION

The demand for creating desired states of light using fully integrated nanostructures has led to the development of metasurfaces (MSs), which rely on the interference of light from engineered scatterers and are composed of ultra-flat planar metallic nanostructures.^{1,2} These structures have nanoscale dimensions and allow engineering of the direction and the relative phase of the scattered light to an unprecedented degree. Based on the Huygens principle, an ensemble of such scatterers can be employed in order to create almost any desired beam shape via superposition, since each MS element can be considered as a dipole-type source of an elementary wave.³ One particular striking feature of MSs is the emergence of a phase-gradient along the MS, leading to generalized forms of the laws of refraction and reflection.³ Due to advances in nanostructuring technology, MSs are used in various fields of photonics, examples of which include sophisticated polarization and beam control,⁴ the observation of the photonic spin Hall effect,^{5,6} ultra-flat lenses,^{7–10} and the generation of orbital angular momentum states.^{11–13} Very recent developments in the field include MSs made from non-metallic materials, leading, for instance, to all-dielectric ultra-flat lenses^{14–16} or for optical cloaks¹⁷ or novel geometries such as catenary MSs.¹⁸

^aAuthor to whom correspondence should be addressed. Electronic mail: henrik.schneidewind@leibniz-ipht.de



One class of widely used MSs is nanoboomerangs having identical two arms with subwavelength lengths and widths and defined opening angles. Compared to other MS geometries such as rotated nanoantennas¹⁹ or structures with sophisticated shapes and materials,^{20,21} the nanoboomerang geometry presents an excellent compromise between fabrication complexity and plasmonic resonance tunability.² The basic working principle of the nanoboomerang geometry relies on a hybridization of the longitudinal localized surface plasmon resonance (LSPR) of the isolated arm,^{4,22,23} resulting in two new non-degenerated eigenstates with antenna resonances at two different wavelengths, whereas the resonance wavelengths are mainly determined by the opening angle and arm length. Associating each eigenstate with a dipole Lorentzian oscillator, the superposition of both oscillators allows engineering phase *and* amplitude almost independently within the spectral interval between the two resonances, which cannot be achieved in non-hybridized structures such as simple bars.

For many applications, it is important that the MS allows access to phases between $-\pi$ and $+\pi$. This is typically achieved by appropriately designing the elements in order to cover the phase space from $-\pi$ to 0 and symmetrically rotating half of the elements by 180° or by an appropriate mirror operation to reach the remaining phases. Due to symmetry reasons, the rotation operation only affects the phase of the crossed polarization state, i.e., the state orthogonal to the input polarization. In our samples, the nanoboomerangs are arranged in a square lattice with their symmetry axes oriented 45° relative to the lattice axes (Fig. 1). Simulations and measurements include an input polarization state parallel to one of the lattice axes (defined as x-axis). Due to the scattering of the elements, the output light contains both parallel and crossed polarized contributions, which are defined as x-state and y-state, respectively. The phases of the parallel state, however, remain unaffected by the rotation operation, and as a consequence the full phase space cannot be accessed when operating in parallel polarization. Ideally, all elements should have identical and strong scattering amplitudes for the crossed polarization state and small amplitudes for the parallel state in order to make the crossed state dominant.

For a MS to operate in reflection, the mentioned conditions are typically achieved using bar-type MSs (here referred as positive MS, meaning pMS), thus isolated scattering elements forming a MS with comparably low metal filling fraction. If transmission mode operation is demanded, however, the low metal filling fraction leads to dominant scattering amplitudes of the parallel polarization state which are stronger than those of the crossed state due to the contribution of the light passing through the non-patterned regions (e.g., Figs. 2(a) and 4(b)). Hence, pMS is problematic to operate in transmission, which is the desirable operation mode for many applications.

According to Babinet's theorem, inverse metasurfaces (iMSs) consisting of slit-type elements can show identical scattering properties as the respective positive structures with the advantage of blocking the non-scattered fraction of the transmitted light. Inverse structures have been fabricated and investigated with regard to applications such as creation and characterization of orbital angular

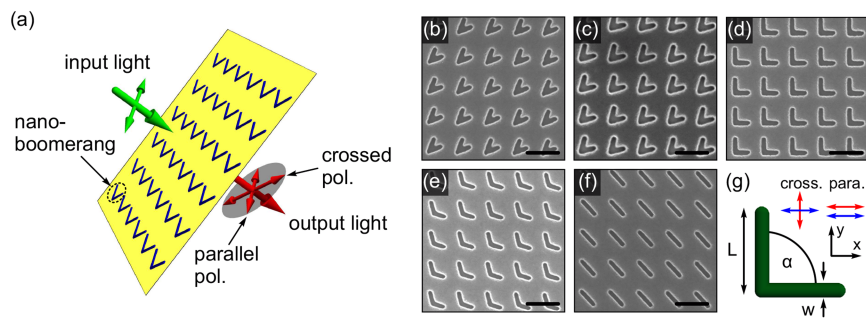


FIG. 1. (a) Schematic of a periodic array of identical inverse metasurface elements (yellow: metal surface, blue: trenches in the metal film providing the iMS). The large (small) arrows indicate the direction (polarization) of the light (green: input, red: output). (b)–(f) Examples of scanning-electron-micrograph images of inverse metasurface structures with various opening angles ((b): 45° , (c): 60° , (d): 90° , (e): 120° , (f): 180°). The scale bar in each image refers to 800 nm. (g) General schematic of the nanoboomerang geometry with the various parameters.

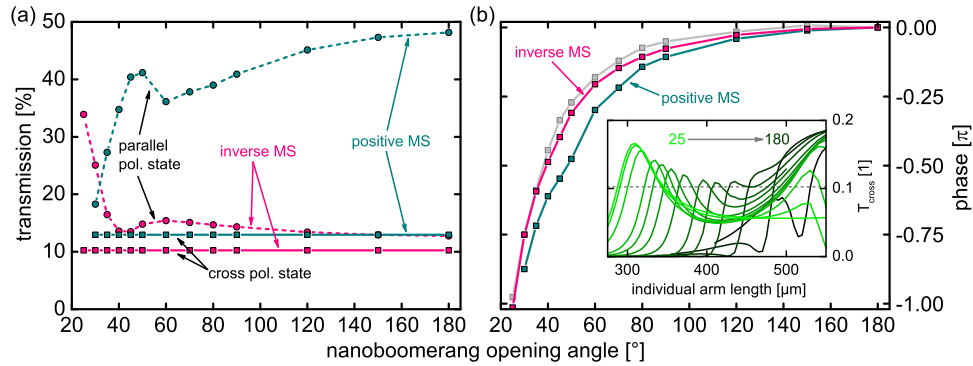


FIG. 2. Comparison of simulation results of the various elements of an optimized inverse metasurface with the corresponding positive structures (constant wavelength: $1.55 \mu\text{m}$). (a) Transmission in the crossed (solid lines, squares) and parallel (dashed lines, circles) polarized states for inverse (pink) and corresponding positive (dark cyan) elements as a function of the nano-boomerang opening angle (parameters). (b) Corresponding phase distribution of the crossed polarized states. The lengths of the nano-boomerang arms have been chosen such that the transmission level in the crossed and parallel polarized states gives 0.10 and 0.13, respectively. The light gray curve corresponds to simulations using non-periodic perfect-matched layer boundary conditions. All phase curves have been shifted by an offset value to yield a zero phase for $\alpha = 180^\circ$. The inset illustrates the optimization procedure and refers to the dependence of the transmission in the crossed polarized state of the individual element on the arm length (each curve refers to one opening angle from left (light green) to right (dark green): $\alpha = 25^\circ, 30^\circ, 35^\circ, 40^\circ, 45^\circ, 50^\circ, 60^\circ, 70^\circ, 80^\circ, 90^\circ, 120^\circ, 150^\circ, 180^\circ$).

momentum modes,^{10,24} implementation of various kinds of elements for polarization discrimination,^{25–27} elements with chiral or holographic properties,^{28,29} and devices for focussing and shaping of beams.^{29–32} Slot-type nano-boomerangs have been used for electro-optical switching.³³ A comparable approach was used in the terahertz frequency region for planar electric split ring resonators.³⁴

Here we show that the individual elements of iMS geometry being composed of slot-type nano-boomerangs with feature sizes of about 100 nm and a high metal filling fraction fulfill the abovementioned conditions for the case of transmission mode operation (Fig. 1(a)). The comparably high metal filling fraction efficiently blocks the undesired contribution of the parallel polarization state, leading to transmission values of the crossed state of the same order as or even slightly higher than that of the parallel state. By conducting a straightforward designing procedure, we show that iMSs being composed of inverse nano-boomerangs allow accessing the entire phase space of 2π , providing identical functionalities as the pMS with substantially improved polarization extinction.

SIMULATION AND OPTIMIZATION PROCEDURE

The elements of the iMSs considered in this work are formed by nanostructured thin metallic films (thickness 60 nm) on a silica substrate. The individual iMS element (i.e., nano-boomerangs, Fig. 1(a)) is formed by two identical slots with one joined edge of defined width and length penetrating the entire film. Here we assume the film to be made from gold, which is a widely used plasmonic metal due to several advantages particular from the application and fabrication perspective.^{35–37} We assumed a constant slot width of 120 nm, which is straightforwardly accessible with our fabrication technology. In order to desirably tune the transmission and phase of each element, i.e., to control the plasmonic hybridization of the longitudinal LSPRs, each single element of the iMS has an independent arm length L and a defined opening angle α . To optimize the structure for a fixed wavelength (here: $1.55 \mu\text{m}$), we performed a scattering analysis using finite element simulations yielding amplitude and phase of the transmitted light (with respect to the input phase) for any combination of the structural parameter in either a crossed or parallel polarization state. The simulations include one unit cell of a single nano-boomerang with periodic and four-port boundary conditions below and above the structure. As only the relative phase between the elements is relevant, we have added an offset value to the phase such as to obtain a zero crossed-polarized phase for an opening angle of $\alpha = 180^\circ$. This geometry

imposes a plane wave excitation and allows obtaining the transmission and reflection amplitudes of the parallel and crossed polarized light.

The main advantages of using nanoboomerangs are the two main geometric parameters (arm length and opening angle) allowing to adjust amplitude and phase of the crossed polarized wave independently. In detail, we simulated the scattering properties for a number of opening angles from 25° to 180° and arm lengths between 250 and 550 nm (the inset of Fig. 2(b)). From this data set, we obtained the maximum amplitude that is possible for all opening angles (gray dashed line in the inset of Fig. 2(b)). If we select the arm lengths corresponding to this selected amplitude value for all opening angles, we obtain a set of nanoboomerangs having the same amplitude for the crossed state covering a phase range of π .

For the iMS geometry considered here (gold film with thickness 60 nm, air slot width 120 nm), the above outlined optimization procedure reveals that accessing the full half phase space from $-\pi$ to 0 is indeed possible at a transmission level of 10% (solid pink lines and purple squares in Figs. 2(a) and 2(b)) in the crossed-polarized state. Except for very small opening angles ($\alpha < 30^\circ$), the transmission of the parallel polarization state is roughly of the same order. This situation is dramatically different in the corresponding pMS, which was optimized using again the mentioned two-step process (metal strip width: 120 nm, gold thickness 60 nm). The procedure yields a pMS showing a maximum transmission of 13% in the crossed state (Fig. 1(b)), being roughly equal to that of the iMS. The transmission in the parallel state, however, is substantially higher for almost all opening angles (dashed dark cyan line in Fig. 2(a)), reaching values being up to four times larger than that of the crossed state. This clearly emphasizes that iMSs are favorable if operation in the transmission mode is considered, since this geometry effectively suppresses the parallel polarization state. The crossed polarization state is therefore more pronounced in an iMS, whereas its impact can diminish in pMS structures. In non-periodic MS arrangements (e.g., geometries including phase gradients), the result from the simulation with periodic boundary conditions can be used by assuming that the total scattered field is the superposition of the fields of the elements, with the individual element characterized by its dipole moment. In order to confirm the validity of our results with respect to non-periodic boundary conditions, we calculated the crossed-polarized phase (in the far-field) of single isolated nanoboomerang elements using a simulation volume surrounded by perfectly matched layers yielding a phase distribution similar to that of the periodic boundary simulations (light gray curve in Fig. 2(b)).

FABRICATION AND MEASUREMENT

In order to investigate the concept of the iMS from the experimental perspective, we implement slot-type nanoboomerangs using a combination of thin film deposition, electron-beam lithography, and ion beam etching. After depositing a 60 nm thick gold film on a planar silica substrate (including a thin titanium adhesion layer), the pattern was written in a 150 nm thin e-beam resist (AR6200.09, ALLRESIST GmbH, Berlin) using e-beam lithography (Vistec SB350 OS). The SB350 OS system operates at 50 keV, leading to accurately positioned and fast exposures down to sub-100 nm structures on wafer-scale areas.³⁸ After developing (60s in AR600-546 and stopped in isopropyle alcohol), the resist pattern was transferred into the gold film by using Ar⁺-ion beam etching (IBE). The residual resist was removed by solvent (AR600-700), followed by a short oxygen-plasma cleaning step (RIE). Scanning-electron microscopy (SEM) revealed an over-etching of the silica substrate by about 30 nm because of the non-selective nature of the IBE.

The resulting structures consist of arrays of identical nanoboomerangs in a square arrangement (array size: 1 mm \times 1 mm, number of identical elements: 1250 \times 1250) with an inter-element pitch of 800 nm (examples of various iMS are shown in Figs. 1(b)–1(f)). The elements of the different arrays have identical air slot width (approximately 120 nm) but various discrete opening angles and engineered arm lengths (of the order of 400 nm) in order to obtain high transmission and large phase angle variations in the crossed-polarized state according to the optimization procedure outlined above. We have fabricated five different arrays with the following opening angles/arm lengths (value refers to α / L): $45^\circ/440$ nm, $60^\circ/455$ nm, $90^\circ/455$ nm, $120^\circ/390$ nm, $180^\circ/320$ nm (widths between 100 nm and 130 nm). To protect the nanostructures from environmental influences, they were covered

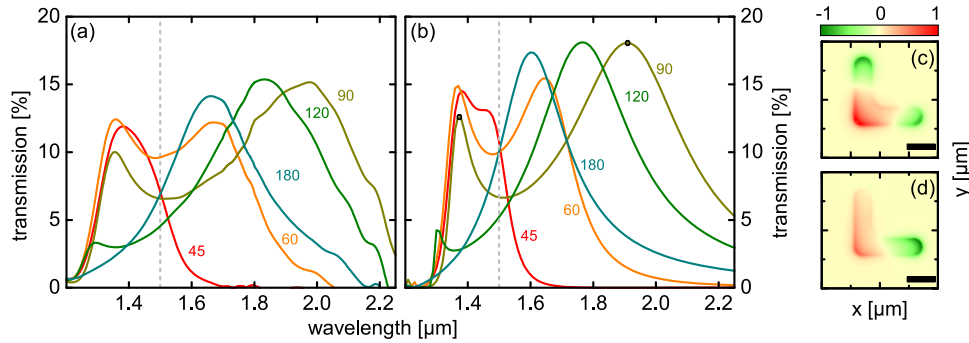


FIG. 3. Spectral distribution of the transmission in the crossed-polarization state for the five different arrays of nanoboomerangs (numbers indicate the opening angle of the different structures, (a): experimental data, (b): finite element simulations). The vertical gray dashed lines in both diagrams indicate the operation wavelength ($1.5 \mu\text{m}$) of our structure. The right-handed images ((c) and (d)) show the spatial near field distributions of the magnetic field component perpendicular to the surface (H_z) of the nanoboomerang modes with $\alpha = 90^\circ$, 5 nm above the film surface at the two resonance wavelengths (top: $\lambda = 1.38 \mu\text{m}$, bottom: $\lambda = 1.91 \mu\text{m}$). The top color bar refers to the normalized amplitude of the H_z component. The black bars in both images indicate a length of 200 nm. Both wavelengths are indicated by the dots in (b) and the color scale ranges from positive (red) to negative values (green).

with a 10 nm thick Al_2O_3 protection layer using atomic layer deposition.³⁹ Preliminary simulations and measurements showed that this layer had negligible influence on the optical properties of the nanoboomerangs, i.e., on the hybridization of the LSPRs. For comparison, we also fabricated elements of a pMS structure using a lift-off process, resulting in nanostructures with a metal strip width of approximately 110 nm and various opening angles and arm lengths.

In order to spectroscopically characterize our nanoboomerangs, we measured the spectral distribution of the transmission between $1 \mu\text{m}$ and $2.4 \mu\text{m}$ using a Perkin-Elmer dual beam spectrometer (sample oriented normal to light beam). Precise control over the crossed and parallel polarization states was ensured by two adjustable polarizers before and after the sample. The extinction of the first polarizer has no influence on the measurement because of an identical polarizer included in the reference beam at equal orientation. The analyzing polarizer in the sample beam has a polarization contrast between 500 and 800 across the spectral interval of interest. In order to evaluate the influence of the absorption of all optical elements within the beam path of the spectrometer (e.g., polarizers), a baseline corresponding to 100% transmission was measured without the sample for normalization purpose. Furthermore, the dark currents of the detectors were recorded by a measurement with both beams blocked. Intensity fluctuations and the light spectral source characteristic were automatically removed from the data by internal normalization using the intensity of the reference beam. In order to account for the Fresnel reflection at the various interfaces and to obtain the transmission of the arrays only, we normalize the transmission that measured at a non-structured part of the sample (without gold) in parallel polarization configuration.

The crossed polarized measurements revealed that all five arrays have a peak transmission between 10% and 15% (Fig. 3). All curves show a clear indication of two Lorentzian oscillator-type resonances, whereas the resonance on the blue side of the spectrum moves towards shorter wavelength with decreasing resonance amplitude for larger opening angles. Note that for $\alpha = 180^\circ$, only one resonance is visible. The resonance on the red side, however, remains at a high level for all geometries, whereas a maximum resonance wavelength is reached for the structure with $\alpha = 90^\circ$.

DISCUSSION

A direct comparison revealed a very close match between simulation and experiment for all nanostructures across the spectral domain of interest (Figs. 3(a) and 3(b)). Particularly remarkable is the close overlap between the resonance wavelength and the associated transmission, indicating the high quality of the fabricated nanostructures. The appearance of two spectrally separated resonances

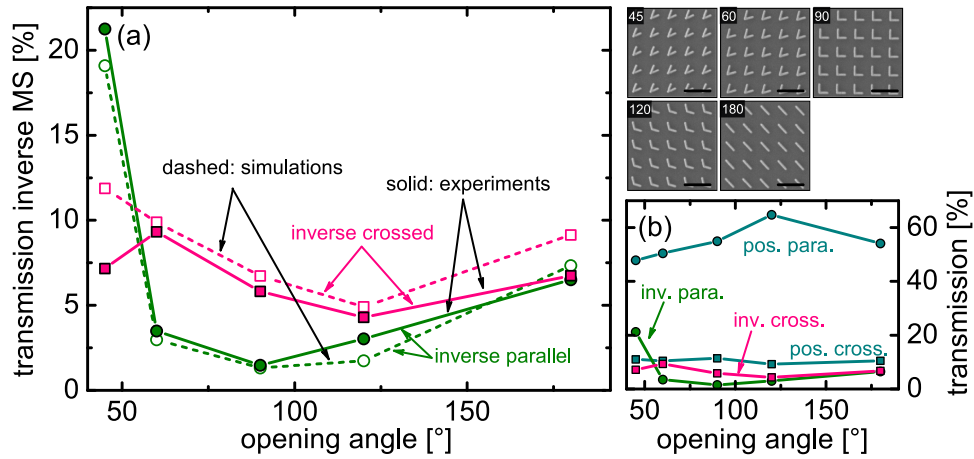


FIG. 4. (a) Transmission level of the fabricated nanoboomerang arrays in crossed (pink) and parallel (green) polarization states at a wavelength of $1.5\ \mu\text{m}$ (solid lines/filled symbols: experimental data, dashed lines/open symbols: finite element simulations using geometrical dimensions of the fabricated samples). (b) shows corresponding measurements of positive structures (wavelength $1.5\ \mu\text{m}$) optimized with the procedure mentioned in the text. The simulations include the 30 nm over-etching into the substrate and the precise dimensions of the fabricated nanoboomerangs, which are slightly different from those associated with Fig. 2. The inset shows SEM images of the pMS arrays (black scale bars refer to 800 nm).

clearly demonstrates the plasmonic hybridization effect within the nanoboomerang geometry (two exemplary intensity distributions are shown in the right-handed images of Fig. 3). It is important to note that the simulations include the real physical dimensions of the nanoboomerangs (given in the above text) and the mentioned 30 nm over-etching into the substrate. The over-etching in fact leads to a blue shift of the hybridized resonances, as otherwise the simulated resonance would be located about 30-80 nm towards longer wavelength (depending on the opening angle).

In order to confirm the superior operation of slot-type nanoboomerang-based iMSs in transmission, we compare the transmission values of both crossed and parallel polarization states at a fixed wavelength of $1.5\ \mu\text{m}$ (crossed (parallel) state: pink (green) curve in Fig. 4). The simulations were performed by taking into account the mentioned 30 nm over-etching into the substrate glass and using the exact geometrical dimensions of the fabricated samples, which are slightly different from those of the nanoboomerangs discussed in Fig. 2. Except for very small values of α , the transmission in the crossed polarization state lies within the interval between 5% and 10% and is higher than that of the parallel state, with the transmission values being fully reproduced by simulations. The increase of the transmission in the parallel state for $\alpha = 45^\circ$ which we attribute to fabrication inaccuracies, as a detailed SEM analysis showed that the inside-section of the nanoboomerang connecting the two arms is particularly vulnerable to such fabrication-induced uncertainties. A direct comparison to the corresponding experimental data of optimized arrays of pMS elements (arm width approximately 100-120 nm, the inset of Fig. 4 showing SEM images) shows the superior property of the iMS geometry of having a higher transmission in the crossed polarization state, which yields a four times improvement in the polarization extinction.

CONCLUSION

In this work, we show the superior properties of inverse metasurfaces compared to their positive counterparts in case the transmission mode operation is considered. The key advantage of such slot-type nanostructures is the strong suppression of transmitted light in the parallel-polarization state, making the crossed-polarization state, which is the relevant state for metasurface operation, highly visible. In the example of nanoboomerangs, we present an optimization procedure to simultaneously obtain high and constant transmission levels of the various metasurface elements while accessing the full phase space. An up to four times improvement in polarization extinction is observed for various elements of the inverse metasurface geometry. We experimentally verified our approach by

implementing a series of nanostructures with feature sizes of the order of 100 nm and determined their spectral characteristics to be polarization-sensitive. The fabricated metasurface elements show the plasmonic hybridization effect, i.e., two spectrally separated resonances, which is the key for the phase and transmission engineering properties of metasurfaces in general. The experiments closely match corresponding simulations and indeed confirm the fourfold improvement in the polarization extinction of inverse metasurface geometry.

Since our presented metasurface concept operates at 1.5 μm , a large number of ultra-flat monolithic photonic elements for applications in telecommunications can be envisioned. Here, the inverse metasurface concept can provide a solid solution to form nanoscale elements such as lenses or devices with ultra-small footprints to generate, e.g., sophisticated states of polarization and beam shapes. To extend the application range of inverse metasurfaces even further, future studies will aim to reduce feature sizes to reach the visible spectral domain for the implementation of, e.g., metalenses⁴⁰ or holographic ultra-flat photonic elements,^{41,42} which both are of particular interest for biophotonics, sensing, or spectroscopy. In the next step, we plan to directly measure the predicted phases of the fabricated nanoboomerangs (e.g., as conducted by Huang *et al.*⁴³) to verify the presented concept of transmission mode operation using inverse metasurface structures.

ACKNOWLEDGMENTS

This work was funded by the Thuringian State Ministry for Economics, Labor, and Technology (Project No. 2012FGR0013) supported by the European Social Funds (ESF).

- ¹ N. F. Yu and F. Capasso, "Flat optics with designer metasurfaces," *Nat. Mater.* **13**, 139–150 (2014).
- ² A. V. Kildishev, A. Boltasseva, and V. M. Shalaev, "Planar photonics with metasurfaces," *Science* **339**, 1232009 (2013).
- ³ N. Yu, P. Genevet, M. A. Kats, F. Aieta, J.-P. Tetienne, C. Capasso, and Z. Gaburro, "Light propagation with phase discontinuities: Generalized laws of reflection and refraction," *Science* **334**, 333–337 (2011).
- ⁴ J. Lin, J. P. Balthasar Mueller, Q. Wang, G. Yuan, N. Antoniou, X.-C. Yuan, and F. Capasso, "Polarization-controlled tunable directional coupling of surface plasmon polaritons," *Science* **340**, 331–334 (2013).
- ⁵ X. Yin, Z. Ye, J. Rho, Y. Wang, and X. Zhang, "Photonic spin Hall effect at metasurfaces," *Science* **339**, 1405–1407 (2013).
- ⁶ Y. Li, Y. Liu, X. Ling, X. Yi, X. Zhou, Y. Ke, H. Luo, S. Wen, and D. Fan, "Observation of photonic spin Hall effect with phase singularity at dielectric metasurfaces," *Opt. Exp.* **23**, 1767–1774 (2015).
- ⁷ X. Chen, L. Huang, H. Mühlenbernd, G. Li, B. Bai, Q. Tan, G. Jin, C.-W. Qui, S. Zhang, and T. Zentgraf, "Dual-polarity plasmonic metalens for visible light," *Nat. Commun.* **3**, 1198 (2012).
- ⁸ W. Wang, Z. Guo, R. Li, J. Zhang, Y. Liu, X. Wang, and S. Qu, "Ultra-thin, planar, broadband, dual-polarity plasmonic metalens," *Photonics Res.* **3**, 68–71 (2015).
- ⁹ F. Aieta, P. Genevet, M. A. Kats, N. Yu, R. Blanchard, Z. Gaburro, and F. Capasso, "Aberration-free ultrathin flat lenses and axicons at telecom wavelengths based on plasmonic metasurfaces," *Nano Lett.* **12**, 4932–4936 (2012).
- ¹⁰ F. Aieta, M. A. Kats, P. Genevet, and F. Capasso, "Multiwavelength achromatic metasurfaces by dispersive phase compensation," *Science* **347**, 1342–1345 (2015).
- ¹¹ E. Karimi, S. A. Schulz, I. De Leon, H. Qassim, J. Upham, and R. W. Boyd, "Generating optical orbital angular momentum at visible wavelengths using a plasmonic metasurface," *Light: Sci. Appl.* **3**, e167 (2014).
- ¹² C.-F. Chen, C.-T. Ku, Y.-H. Tai, P.-K. Wei, H.-N. Lin, and C.-B. Huang, "Creating optical near-field orbital angular momentum in a gold metasurface," *Nano Lett.* **15**, 2746–2750 (2015).
- ¹³ W. Wang, Y. Li, Z. Guo, R. Li, J. Zhang, A. Zhang, and S. Qu, "Ultra-thin optical vortex phase plate based on the metasurface and the angular momentum transformation," *J. Opt.* **17**, 45102–45108 (2015).
- ¹⁴ F. Zhang, H. Yu, J. Fang, M. Zhang, S. Chen, J. Wang, A. He, and J. Chen, "Efficient generation and tight focusing of radially polarized beam from linearly polarized beam with all-dielectric metasurface," *Opt. Exp.* **24**, 6656–6664 (2016).
- ¹⁵ J. Zhong, N. An, N. Yi, M. Zhu, Q. Song, and S. Xiao, "Broadband and tunable-focus flat lens with dielectric metasurface," *Plasmonics* **11**, 537–541 (2016).
- ¹⁶ B. J. Bohn, M. Schnell, M. A. Kats, F. Aieta, R. Hillenbrand, and F. Capasso, "Near-field imaging of phased array metasurfaces," *Nano Lett.* **15**, 3851–3858 (2015).
- ¹⁷ L. Y. Hsu, T. Lepetit, and B. Kanté, "Extremely thin dielectric metasurface for carpet cloaking," *Prog. Electromagn. Res.* **152**, 33–40 (2015).
- ¹⁸ X. Li, M. Pu, Z. Zhao, X. Ma, J. Jin, Y. Wang, P. Gao, and X. Luo, "Catenary nanostructures as compact Bessel beam generators," *Sci. Rep.* **6**, 20524 (2016).
- ¹⁹ L. Huang, X. Chen, H. Mühlenbernd, G. Li, B. Bai, Q. Tan, G. Jin, T. Zentgraf, and S. Zhang, "Dispersionless phase discontinuities for controlling light propagation," *Nano Lett.* **12**, 5750–5755 (2012).
- ²⁰ S. Sun, K.-Y. Yang, C.-M. Wang, T.-K. Juan, W. T. Chen, C. Y. Liao, Q. He, S. Xiao, W.-T. Kung, G.-Y. Guo, L. Zhou, and D. P. Tsai, "High-efficiency broadband anomalous reflection by gradient meta-surfaces," *Nano Lett.* **12**, 6223–6229 (2012).
- ²¹ C. Pfeiffer and A. Grbic, "Metamaterial Huygens' surfaces: Tailoring wave fronts with reflectionless sheets," *Phys. Rev. Lett.* **110**, 197401 (2013).
- ²² D. Vercrusse, Y. Sonnefraud, N. Verellen, F. B. Fuchs, G. Di Martino, L. Lagae, V. V. Moshchalkov, S. A. Maier, and P. Van Dorpe, "Unidirectional side scattering of light by a single-element nanoantenna," *Nano Lett.* **13**, 3843–3849 (2013).

- ²³ M. A. Kats, P. Geneveta, G. Aousta, N. Yua, R. Blanchard, F. Aieta, Z. Gaburro, and F. Capasso, "Giant birefringence in optical antenna arrays with widely tailorable optical anisotropy," *PNAS* **109**, 12364–12368 (2012).
- ²⁴ J. Jin, J. Luo, X. Zhang, H. Gao, X. Li, M. Pu, P. Gao, Z. Zhao, and X. Luo, "Generation and detection of orbital angular momentum via metasurface," *Sci. Rep.* **6**, 24286 (2016).
- ²⁵ R. Li, Z. Guo, W. Wang, J. Zhang, A. Zhang, J. Liu, S. Qu, and J. Gao, "High-efficiency cross polarization converters by plasmonic metasurface," *Plasmonics* **10**, 1167–1172 (2015).
- ²⁶ P. Mandal, S. A. Ramakrishna, R. Patil, and A. V. Gopal, "Polarization dependent color switching by extra-ordinary transmission in H-slit plasmonic metasurface," *J. Appl. Phys.* **114**, 224303 (2013).
- ²⁷ C. Pelzman and S.-Y. Cho, "Polarization-selective optical transmission through a plasmonic metasurface," *Appl. Phys. Lett.* **106**, 251101 (2015).
- ²⁸ Y.-P. Jia, Y.-L. Zhang, X.-Z. Dong, M.-L. Zheng, J. Li, J. Liu, Z.-S. Zhao, and X.-M. Duan, "Complementary chiral metasurface with strong broadband optical activity and enhanced transmission," *Appl. Phys. Lett.* **100**, 011108 (2014).
- ²⁹ R. Li, Z. Guo, W. Wang, J. Zhang, K. Zhou, J. Liu, S. Qu, S. Liu, and J. Gao, "Arbitrary focusing lens by holographic metasurface," *Photon. Res.* **3**, 252–255 (2015).
- ³⁰ X. Ni, S. Ishii, A. V. Kildishev, and V. M. Shalaev, "Ultra-thin, planar, Babinet-inverted plasmonic metalenses," *Light: Sci. Appl.* **2**, e72 (2013).
- ³¹ S. Wang, D. C. Abeysinghe, and Q. Zhan, "Generation of vectorial optical fields with slot-antenna-based metasurface," *Opt. Lett.* **40**, 4711–4714 (2015).
- ³² D. Wen, F. Yue, M. Ardon, and X. Chen, "Multifunctional metasurface lens for imaging and Fourier transform," *Sci. Rep.* **6**, 27628 (2016).
- ³³ Y. U. Lee, J. Kim, J. H. Woo, L. H. Bang, E. Y. Choi, E. S. Kim, and J. W. Wu, "Electro-optic switching in phase-discontinuity complementary metasurface twisted nematic cell," *Opt. Exp.* **22**, 20816–20827 (2014).
- ³⁴ H.-T. Chen, J. F. O'Hara, A. J. Taylor, R. D. Averitt, C. Highstreet, M. Lee, and W. J. Padilla, "Complementary planar terahertz metamaterials," *Opt. Exp.* **15**, 1084–1095 (2007).
- ³⁵ R. Alaei, C. Menzel, U. Huebner, E. Pshenay-Severin, S. Bin Hasan, T. Pertsch, C. Rockstuhl, and F. Lederer, "Deep-subwavelength plasmonic nanoresonators exploiting extreme coupling," *Nano Lett.* **13**, 3482–3486 (2013).
- ³⁶ T. Wieduwilt, A. Tuniz, S. Linzen, S. Goerke, J. Dellith, U. Huebner, and M. A. Schmidt, "Ultrathin niobium nanofilms on fiber optical tapers—A new route towards low-loss hybrid plasmonic modes," *Sci. Rep.* **5**, 17060 (2015).
- ³⁷ H. W. Lee, M. A. Schmidt, and P. St. J. Russell, "Excitation of a nanowire 'molecule' in gold-filled photonic crystal fiber," *Opt. Lett.* **37**, 2946–2948 (2012).
- ³⁸ U. Huebner, M. Falkner, U. D. Zeitner, M. Banasch, K. Dietrich, and E. B. Kley, "Multi-stencil character projection e-beam lithography: A fast and flexible way for high quality optical metamaterials," *Proc. SPIE* **9231**, 92310E (2014).
- ³⁹ S. Yüksel, M. Ziegler, S. Goerke, U. Huebner, K. Pollok, F. Langenhorst, K. Weber, D. Cialla-May, and J. Popp, "Background-free bottom-up plasmonic arrays with increased sensitivity, specificity and shelf life for SERS detection schemes," *J. Phys. Chem. C* **119**, 13791–13798 (2015).
- ⁴⁰ M. Khorasaninejad, W. T. Chen, R. C. Devlin, J. Oh, A. Y. Zhu, and F. Capasso, "Metalenses at visible wavelengths: Diffraction-limited focusing and subwavelength resolution imaging," *Science* **352**, 1190–1194 (2016).
- ⁴¹ G. Zheng, H. Mühlenbernd, M. Kenney, G. Li, T. Zentgraf, and S. Zhang, "Metasurface holograms reaching 80% efficiency," *Nat. Nanotechnol.* **10**, 308–312 (2015).
- ⁴² Y.-W. Huang, W. T. Chen, W.-Y. Tsai, P. C. Wu, C.-M. Wang, G. Sun, and D. P. Tsai, "Aluminum plasmonic multicolor meta-hologram," *Nano Lett.* **15**, 3122–3127 (2015).
- ⁴³ Y.-W. Huang, H. W. H. Lee, R. Sokhoyan, R. A. Pala, K. Thyagarajan, S. Han, D. P. Tsai, and H. A. Atwater, "Gate-tunable conducting oxide metasurfaces," *Nano Lett.* **16**, 5319–5325 (2016).